Title

Mechanics of the energy balance in large lowland rivers, and why the bed matters

Journal

Geophysical Research Letters, 44(17)

ISSN

0094-8276

Authors

Bray, Erin N
Dozier, Jeff
Dunne, Thomas

Publication Date

2017-09-16

DOI

10.1002/2017gl075317

Peer reviewed

AGU PUBLICATIONS

Geophysical Research Letters

RESEARCH LETTER
10.1002/2017GL075317

Key Points:
- A full-spectrum fluvial energy balance model shows river temperature depends on depth, the spectral distribution of sunlight, and bed albedo
- Sand to gravel variations in bed sediment albedo can alter the energy balance and river temperature by up to 2°C
- Plausible releases of cold water from a dam cool the river for no more than tens of kilometers downstream

Supporting Information:
- Supporting Information S1

Correspondence to:
E. N. Bray,
ebray@bren.ucsb.edu

Citation:
Bray, E. N., J. Dozier, and T. Dunne (2017), Mechanics of the energy balance in large lowland rivers, and why the bed matters, *Geophys. Res. Lett.*, *44*, 8910–8918, doi:10.1002/2017GL075317.

Received 18 AUG 2017
Accepted 19 AUG 2017
Accepted article online 23 AUG 2017
Published online 9 SEP 2017

Mechanics of the energy balance in large lowland rivers, and why the bed matters

Erin N. Bray[1,2], Jeff Dozier[3], and Thomas Dunne[3]

[1]Earth Research Institute, University of California, Santa Barbara, California, USA, [2]Center for Environmental Design Research, University of California, Berkeley, California, USA, [3]Bren School of Environmental Science and Management, University of California, Santa Barbara, California, USA

Abstract Along many rivers, dams trap sediment and water released from the dams is clear. Downstream of the dam, temperature variability along the river is controlled by climate that warms or cools the water, the flow magnitude, and the spectral properties of water and the river's bed. Using field observations, a synoptic numerical model without calibration couples a full-spectrum radiation balance with turbulent heat fluxes, bed conduction, and a hydraulic model that estimates depth and velocity. We show that variations in the river's temperature are sensitive to the albedo of the sediment on the bed, especially at shallow depths and smaller discharges. However, about half the solar radiation lies in a spectral range where water is highly absorptive; in these wavelengths, absorption is independent of depth. In spring and summer with many hours of sunlight, releases of cold water will have limited influence on temperatures beyond tens of kilometers downstream of a dam.

1. Introduction

Partitioning of radiative, sensible, and latent energy exchange into evaporation and absorption in a river depends on the radiation that is absorbed by the water column and the bed, the rate at which energy is added or removed through atmosphere-water surface interactions, and the rate at which the river flow transports and accumulates energy in the water. Thus, climate coupled with advective and diffusive flow processes influences the energy balance of a river, whose thermal dynamics control ecosystem function [*Ward*, 1989], instream primary productivity [*Blinn and Cole*, 1991], biogeochemistry [*Craine et al.*, 2010], and the growth and survival of anadromous and resident fish [*Benjamin et al.*, 2012].

On a clear day, most of the solar radiation S is direct at solar zenith angle θ_i. When S strikes the water surface, some fraction is reflected; the complementary fraction is transmitted and also refracted, so it enters the water column at angle θ_r. At that angle, it passes through the water column to the bed. Some of it is absorbed along the way. The portion reaching the bed either reflects or is absorbed, and some of the reflected portion is absorbed as it travels back to the surface, while some fraction emerges from the surface. The portion that is absorbed, S_{net}, is then available for sensible and latent heat exchange between the water and the atmosphere, advective and diffusive exchange by water moving into or out of the column, conduction into or out of the deeper bed sediment, and for warming the water itself (Figure 1).

The most important optical characteristic of water, which causes spectral variation in absorption and reflection, is that the absorption coefficient k varies by eight orders of magnitude over the solar spectrum [*Hale and Querry*, 1973]. In the infrared spectrum, water is absorptive, so almost all incoming longwave radiation is absorbed. While considerable attention has been paid to variations in the transmission of light for photosynthesis in aquatic ecosystems [*Julian et al.*, 2008; *Kirk*, 2011], thermal regimes in lakes [*Hausner et al.*, 2013], and for measuring river bathymetry from remotely sensed data [*Legleiter et al.*, 2009; *Carbonneau and Piégay*, 2012], previous work commonly defines absorption in water empirically without specification of wavelength [*Kirk*, 2011]. Neglecting the wavelength dependence of solar attenuation masks the effects of the bed's reflectivity and the river's depth on absorption of solar radiation by the water.

As such, several distinctive features of large, regulated rivers are absent from existing models. First, their low gradients and concave profiles make them susceptible to mobilization of sediment, which in turn affects the along-stream variations in channel bed composition [*Dunne and Aalto*, 2013]. Bed material tends be finer in the downstream direction [*Paola and Wilcock*, 1989]. Second, their large drainage areas, climate, lithology,

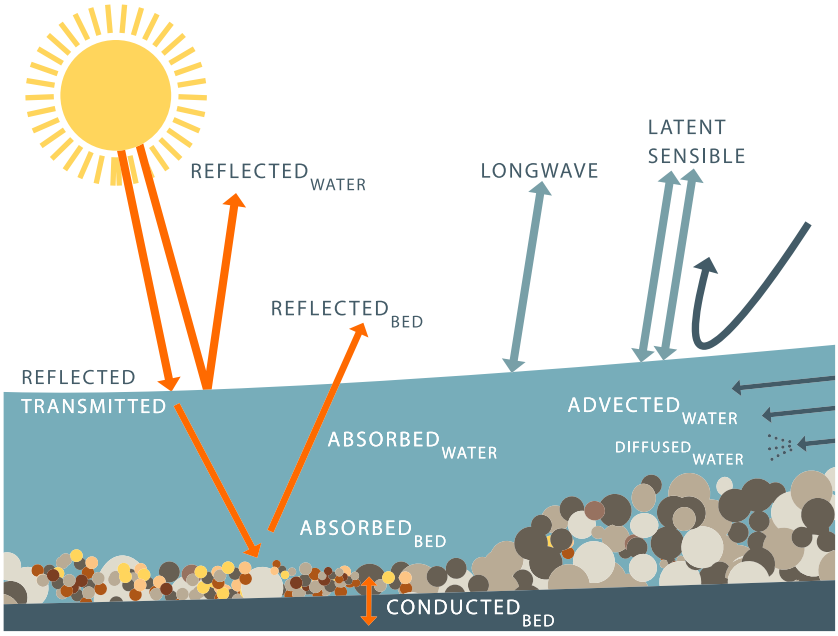

Figure 1. Partitioning of radiative heat over the length of a large lowland river.

and flow management determine the river discharge and sediment load. At a particular discharge, the width, velocity, and depth adjust to satisfy equilibrium related to the slope [*Leopold and Wolman*, 1957], which controls how effectively the river transports heat. Increasing width downstream reduces the degree to which riparian vegetation shades the river. Third, a gravel-to-sand transition is often marked by a discontinuity in slope and morphology, where grain size can decrease abruptly [*Paola et al.*, 1992] or gradually [*Singer*, 2008]. In fluvial environments, gravels have a lower albedo than fine sand [*Legleiter et al.*, 2009]. Lowland rivers have distinctive features that need to be accounted for in predicting their energy balance and temperature: shallow depth at low flows, variation in the albedo of the bed material, and warmer air temperatures as the river flows into the lowlands. An accurate description of the physics of energy exchange in rivers involves a method by which net radiation and turbulent heat fluxes may be calculated at any time or distance over the length of a large river whose hydraulic and sediment characteristics vary as a function of the flow regime and sediment supply. For clear, flowing water that is usually present below dams, we present a fluvial energy balance model that couples a spectral radiation balance with turbulent heat fluxes, bed conduction, and a 1-D hydraulic model employed over the longitudinal profile of a large river whose water depth and velocity vary with distance downstream. The basic governing heat transport equation is [*Sridhar et al.*, 2004]

$$\frac{\partial T}{\partial t}+\frac{v}{Q}\frac{\partial (TQ)}{\partial x}=\frac{Q_{\text{net}}}{\rho c_p D}+\frac{v}{Q}\frac{\partial}{\partial x}\left[D_L\frac{Q}{v}\frac{\partial T}{\partial x}\right] \tag{1}$$

T is average cross-sectional temperature at time t and distance x along the river, v is flow velocity, Q_{net} is the net energy exchange between the atmosphere, the bed, and the water, Q without subscript is river discharge, ρ is water density, c_p is specific heat of the water, D is the depth, and D_L is the longitudinal dispersion coefficient. The water is assumed to be well-mixed.

The model computes radiative absorption through specification of bed albedo and absorption by the water and the bed based on the spectral properties of water and the water depth. In the current context, the model applies to clear water only but could be adapted to rivers with suspended sediment loads or dissolved organic material. We pay detailed attention to the radiative heat transfer and the changes in the energy balance resulting from regulated flow releases and bed composition because these distinctive features can be specified directly from field measurements and because some results of general importance emerge.

2. Theory and Methods

The surface-bed-atmosphere interaction governing the energy balance and thermal regime of a large lowland river is controlled by the net absorption of solar and longwave radiation, the turbulent fluxes of sensible and latent heat, the conduction at the bed, and heat storage in the water column. Energy from the atmosphere and the bed, Q_{net} in W m^{-2}, is

$$Q_{net} = S_{net} + F_{net} + H + L + G \tag{2}$$

S_{net} is the net solar radiation, F_{net} is the net longwave radiation, H is the sensible heat flux, L is the latent heat flux, and G is the bed conduction (Figure 1). The advective component in equation (1), $(v/Q)[\partial(TQ)/\partial x]$, expresses the amount of energy transported along the river. Positive terms in Q_{net} heat the water; all except S_{net} can be negative. Exchanges of energy from longwave radiation and sensible and latent heat fluxes occur at the water surface, but solar radiation heats the water through absorption in the water column—on its way to the bed and after reflection from the bed—and by warming the bed itself, which heats the water column by convection and transfers heat to and from the deeper sediments by conduction. The model assumes vertically homogeneous optical properties and that the water column is fully mixed.

The transmission of solar energy into the water column occurs primarily between wavelengths 0.28 and 4.0 μm. At Earth's surface, the measured solar radiation is the sum of the direct and diffuse components $S = S_0 + S_{dif}$. On clear days most of the radiation is in the direct component at solar zenith angle θ_i. The diffuse component is assumed isotropic. The solar zenith angle may be calculated from the latitudes and longitudes of a location [*Sellers*, 1965]. Although we have measurements of solar radiation at the surface, we assess the validity of those published data by making sure that the surface measurements do not exceed the calculated value above the atmosphere. Accurate approximations to the solar declination, Earth-Sun radius vector, and equation of time are calculated based on equations in the NOAA Solar Calculator (NOAA Earth System Research Laboratory, http://www.esrl.noaa.gov/gmd/grad/solcalc/). Computation of the solar zenith angle includes atmospheric refraction [*Kasten and Young*, 1989]. Solar radiation is either reflected from the water's surface or transmitted into the water column. Surface reflectivity R_{surf} is approximated by averaging the Fresnel reflectivity for perpendicular ($R_\perp$) and parallel ($R_\parallel$) polarized values [*Born and Wolf*, 1959], based on θ_i, the angle of incidence, and n, the real part of the complex index of refraction $n + ik$:

$$R_{surf} = \frac{R_\perp + R_\parallel}{2} = \frac{1}{2}\left[\left(\frac{\cos\theta_i - n\cos\theta_r}{\cos\theta_i + n\cos\theta_r}\right)^2 + \left(\frac{\cos\theta_r - n\cos\theta_i}{\cos\theta_r + n\cos\theta_i}\right)^2\right] \tag{3}$$

Once solar radiation passes through the water surface, it is transmitted toward the bed at the angle of refraction θ_r. In water with little suspended sediment, we neglect scattering from the water volume because scattering from pure water over the depth of the river is negligible. In visible wavelengths, water is transparent, whereas in near-infrared wavelengths it is more opaque. Total transmissivity, the fraction of the incident radiation that reaches the bed, is the product of their values through the surface and then through the water column, i.e., $\psi_{surf} \times \psi_{bed}$. These values depend on the wavelength λ of the light,

$$\begin{aligned} \psi_{surf}(\lambda) &= 1 - R_{surf}(\lambda) \\ \psi_{bed}(\lambda) &= e^{-\tau_0(\lambda)/\cos\theta_r} \end{aligned} \tag{4}$$

Here $\theta_r = \sin^{-1}(n \sin\theta_i)$ is the angle of refraction resulting when radiation is transmitted from one medium to another (air to water), τ_0 is the optical depth, λ is the wavelength of the light, ψ_{surf} is the transmissivity through the surface, ψ_{bed} is the transmissivity to the bed, and $\psi_{surf} \times \psi_{bed}$ is the total transmissivity.

The optical depth, τ_0, of the water column is related to the absorption coefficient k (the imaginary part of the refractive index) and the water depth D, $\tau_0(\lambda) = 4\pi k(\lambda)D/\lambda$. The extinction coefficient $k(\lambda)$ characterizes the absorption properties of a material. For the radiation transmitted in the water in the beam, the length of the optical path from the surface to the bed is $\tau_0/\cos\theta_r$. Of the fraction of the radiation that reaches the streambed $\psi_{surf} \times \psi_{bed}$, a fraction R_{bed} is reflected, the fraction $1 - R_{bed}$ is absorbed. Depending on the magnitude and direction of the temperature gradient in the sediments, some of this energy is transferred into the sediments, or if the gradient is upward, for example, at night, extra energy flows upward from the sediments to the bed. Depending on the direction of the conduction into the bed, energy is either subtracted from or added to Q_{net}. According to *Constantz* [2008], in flowing rivers the temperature adjustment is immediate, so

the water and the bed have the same temperature (which would not be the case in lakes, which are frequently stratified). We assume that R_{bed} is isotropic, so the radiation reflected from the streambed takes a variety of paths back toward the surface. The average optical path is $\pi\tau_0$ (because $\int_0^{2\pi}\left(\int_0^{\pi/2}\sin\theta\cos\theta \mathrm{d}\theta\right)\mathrm{d}\phi = \pi$, where θ and ϕ are the angle and azimuth of the direction of reflection from the bed), so following equation (4), the fraction of the bed-reflected radiation getting back out to the surface is

$$\psi_{back} = e^{-\pi\tau_0} \tag{5}$$

Consolidating these multiple transmissions and reflections in equations (2) through (5), the S_{net} portion of the energy balance in equation (1) has a spectral dependence, most easily estimated by calculating the reflectivity R_{back} of the whole system:

$$\begin{aligned}\frac{S_{net}(\lambda)}{S(\lambda)} &= 1 - R_{back}(\lambda) = 1 - \left(R_{surf} + \psi_{surf}\psi_{bed}R_{bed}\psi_{back}\right)\\ &= \left(1 - R_{surf}\right)\left[1 - R_{bed}e^{-\tau_0(\pi+\sec\theta_r)}\right]\end{aligned} \tag{6}$$

All terms on the right-hand side are spectrally dependent, although R_{bed} is often estimated as spectrally constant. Over the solar spectrum, the absorption coefficient k (and thus $\tau_0(\lambda)$) varies by eight orders of magnitude (Figure S1). We partition the spectrally integrated measured incoming solar radiation into its spectral distribution using published measurements [*Gueymard*, 2004]. We calculate the absorption by the water and streambed at each wavelength and we integrate across the spectrum. Net longwave radiation is the difference between absorbed incoming and emitted outgoing longwave radiation. Downwelling long-wave radiation, $\Phi_{\downarrow}$, is calculated using a clear-sky algorithm [*Prata*, 1996] combined with a cloud correction [*Crawford and Duchon*, 1999], as

$$\Phi_{\downarrow} = \varepsilon_{clr}\sigma {T_a}^4 \tag{7}$$

$$\varepsilon_{clr} = 1 - \left(1 + w_p\right)\exp\left[-\left(1.2 + 3w_p\right)^{1/2}\right] \tag{8}$$

$$\varepsilon_a = (1 - s) + s\varepsilon_{clr} \tag{9}$$

$\Phi_{\downarrow}$ is the incoming long-wave radiation for clear skies, ε_{clr} is the clear-sky emissivity, T_a is air temperature, w_p is the precipitable water in mm, ε_a is the effective atmospheric emissivity, and s is the ratio of actual solar to the clear-sky irradiance. The outgoing radiation emitted from the water surface is a function only of the water temperature T (°K):

$$\Phi_{\uparrow} = \varepsilon\sigma T^4 \tag{10}$$

where ε water emissivity is about 0.97 and σ is the Stefan-Boltzmann constant. Surface thermodynamic fluxes are computed based on bulk aerodynamic methods. *Verburg and Antenucci* [2010] provide considerable detail about the calculations.

$$H = \rho_a c_a C_H U_z (T - T_a) \text{ sensible heat transfer} \tag{11}$$

$$L = \rho_a L_v C_E U_z (q_s - q_a) \text{ latent heat transfer} \tag{12}$$

C_H and C_E are the transfer coefficients for sensible and latent heat, respectively, c_a is the specific heat of air (J kg^{-1} K^{-1}), ρ_a is air density (kg m^{-3}), L_v is the enthalpy of vaporization (J kg^{-1}), T and T_a are the surface and air temperatures, and q_s and q_a are the specific humidity of the surface and air. Streambed conduction G is calculated using an implicit solution for the diffusion equation [*Richtmyer and Morton*, 1967], which solves the temperature for all sediment depth nodes at each time step. With **M** as the transition matrix and **T** as the temperature vector downward from the surface, the equation to solve to get from time t to $t + 1$ is

$$\mathbf{M}\cdot\mathbf{T}_{t+1} = \boldsymbol{T}_t \tag{13}$$

Here **M** is a function of the Fourier modulus $F = \alpha\Delta t/(\Delta s)^2$ where $\alpha = K/(\rho_s c_s)$ is the thermal diffusivity and Δs is the node spacing in the sediment, set at 0.05 m. Values for thermal conductivity $K = 2.4$ W m^{-1} deg^{-1} and volumetric heat capacity $\rho_s c_s = 2.59 \times 10^6$ J m^{-3}deg^{-1}. The sediment's thermal properties are assumed to be constant over the study reach. Therefore, the computation requires inverting **M** only once, so at every time step

$$\mathbf{T}_{t+1} = \boldsymbol{M}^{-1} \cdot \boldsymbol{T}_t. \tag{14}$$

Equation (8) in *Dozier and Outcalt* [1979] shows the equation for **M**. The model estimates temperatures down to 1 m below bed, at which depth the temperature is assumed to not vary over the period of the analyses. The change in water temperature in the river is based on $Q_{\text{net}} \pm$ conduction into the bed, so energy that goes into the bed reduces the warming of the water. Conversely, when this energy comes back out (at night) then it warms the water. Frictional heat generation was computed and determined to be negligible (supporting information). The heat transport equation (equation (1)) is solved by an explicit finite difference scheme [*Sridhar et al.*, 2004]:

$$T_x^{t+1} = T_x^t + \Delta t \left\{ \frac{v_x}{Q_x} \left[-\nabla_x \left(Q_x T_x^t \right) + \nabla_x \left(\frac{Q_x D_{Lx}}{v_x} \nabla_x \left(T_x^t \right) \right) \right] + \frac{{Q_{\text{net}}}_x^{t+1} + {Q_{\text{net}}}_x^t}{2 \rho c_p D} \right\} \tag{15}$$

The variables are the same as in equation (1), with the subscript x and superscript t representing discrete longitudinal distance and time steps. The along-stream gradients ∇_x are calculated by central differences, i.e., $\nabla_x \left(Q_x T_x^t \right) = \left(Q_{x+1} T_{x+1}^t - Q_{x-1} T_{x-1}^t \right) / 2\, \Delta x$. The dispersion coefficient D_L [*Zeng and Huai*, 2014], with u_* as shear velocity, is

$$D_L = 5.4 D v \left(\frac{Q}{D^2 v} \right)^{0.7} \left(\frac{v}{u_*} \right)^{0.13} \tag{16}$$

Because the energy flux term ${Q_{\text{net}}}_x^{t+1}$ contains components that depend on the water temperature at the same time step, an iterative approach is used in combination with the finite difference equation to account for this dependence in the solution. The iteration method [*Sridhar et al.*, 2004] consists of initially assuming $T_x^{t+1} = T_x^t$ and computing the energy term ${Q_{\text{net}}}_x^{t+1}$. The finite difference equation is then solved again giving a new value of T_x^{t+1}, repeating until the solution converges. The convergence criteria used was $\lfloor \Delta T \rfloor \leq 10^{-5}$ K. The analysis is validated with measurements from a robust monitoring network established prior to a large-scale flow experiment in a 150 km reach of the San Joaquin River, California, beginning at Friant Dam (Figure S2). The data span a year of meteorological conditions (2010) and two steady state discharges at 7.8 and 43.3 $m^3\ s^{-1}$, for which spatially distributed values of width, depth, and velocity were modeled with HEC-RAS version 4.1.0 (U.S. Army Corps of Engineers, HEC-RAS, Hydrologic Engineering Center, http://www.hec.usace.army.mil/software/hec-ras/). The energy balance was then simulated with grid spacing of 100 m at a fine enough time step to keep the Courant number no greater than 0.3. The site, data, hydraulic model, and model validation are described in greater detail in the supporting information [*California Department of Water Resources*, 2010].

3. Results

The magnitude of the processes that control partitioning of S across λ between the bed and the water column are shown by the variation in the reflection and absorption spectra for water depths of 0.5 and 5 m (Figure 2). In visible wavelengths, water is transparent so most of the absorption is by the bed, whereas in the near-infrared and thermal infrared wavelengths the water itself absorbs the radiation. At the shallower 0.5 m depth, 38% of the spectrally integrated solar radiation is absorbed by the bed. The corresponding proportion absorbed by the water is 51%, of which only 2% is absorbed on the upward path (Table S1).

The shape of the spectra and magnitude of the transmissions for low and high flow depths are different. As depth D increases, the shape of the absorption and reflection spectra change (Figure 2b) and the fraction absorbed at the bed decreases. Less radiation reaches the bed, more is absorbed in the water, and the importance of the bed properties diminishes. Because radiation that reaches the bed occurs in the wavelengths where water is most transparent, most of the bed-reflected radiation gets out of the water (Table S1). About half of the incoming solar radiation occurs in the visible wavelengths where flow depth and bed albedo matter. In the rest of the spectrum, especially beyond 1 μm, the fraction that is absorbed by the water is essentially independent of depth. When the water is deep, most of the radiation is absorbed in the water, whereas during low flows with a high radiation load, the major contributor to warming the water is the absorption at the bed.

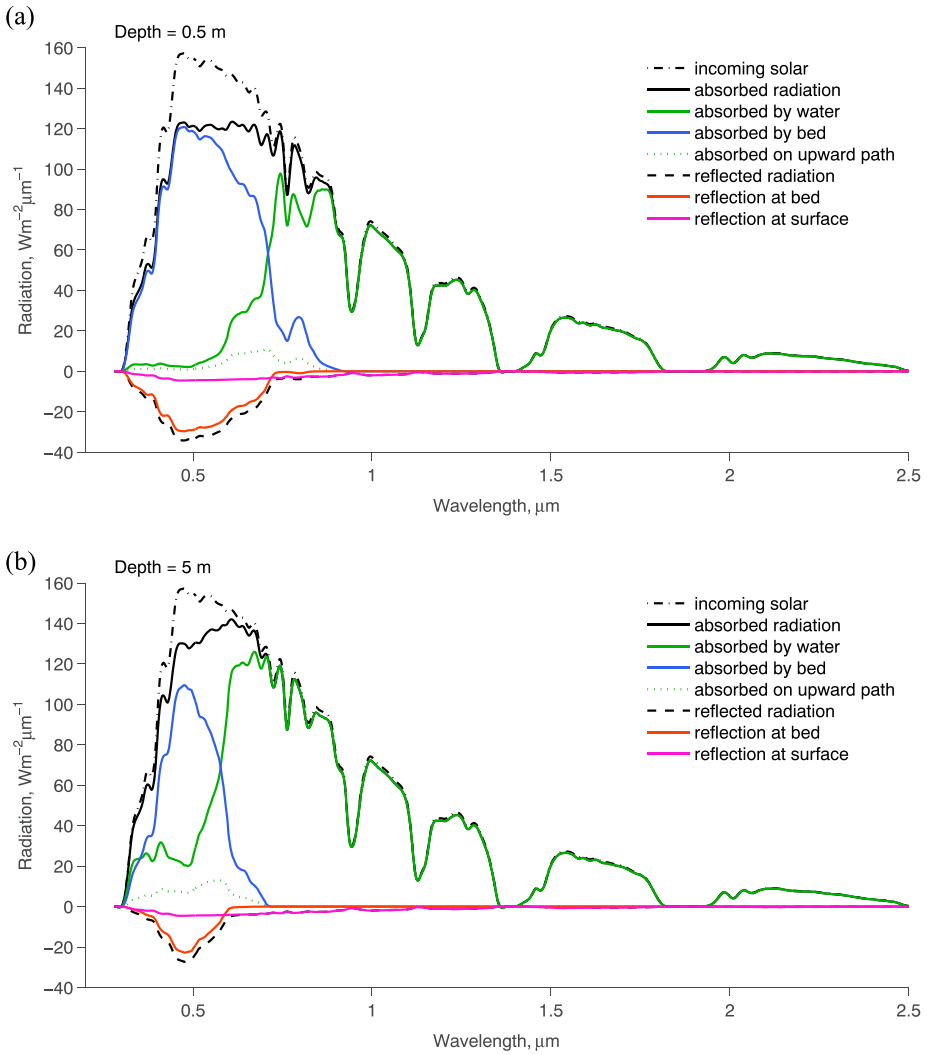

Figure 2. Spectral reflectance and absorption of radiant energy in a river. Transmissions across wavelengths 0.28 to 2.8 μm for water depths of (a) 0.5 m, and (b) 5.0 m assuming S = 100 W m^{-2}, θ_i = 45 degrees and R_{bed} = 0.2. Here there are two phenomena that are convolved: (1) the spectral variability in the optical properties of water and (2) the spectral variability in the solar illumination, so there would be spectral variability in the radiation absorbed and reflected, even if water's optical properties were uniform. Together these combine to produce the actual spectrum of absorption and reflection.

Net absorbed shortwave radiation (S_{net}) and bed albedo (R_{bed}) are of course inversely related (Figure S3a). Direct field measurements have shown that R_{bed} of wet sediment in rivers ranges from 0.04 to 0.5 [*Zhang and Voss*, 2006; *Legleiter et al.*, 2009]. The inverse relationship between S_{net} and R_{bed} implies the following generalities: (1) the systematic downstream fining of sediment frequently observed in large rivers results in a systematic downstream increase in ψ_{back}, the fraction of the bed-reflected radiation, (2) in gravel-bedded reaches, lower R_{bed} increases the overall absorption of energy, and (3) explicitly partitioning the absorption between the water column and streambed improves the understanding of "where" the heating occurs. Heating the water from the bottom can cause mixing, whereas heating the water from the top can cause stratification, though in most flowing rivers the water mixes turbulently [*Fischer et al.*, 2013].

In large rivers, the bed material often ranges from gravel to sand, and this variation in lithology determines the albedo. In gravel-bedded rivers, almost all of the incoming solar radiation is absorbed by the bed or the water regardless of flow depth (Figure S3b). During low flow in a gravel bed, up to half of the total absorbed radiation occurs at the bed rather than in the water column (Table S2). For the same shallow flow in a sandy river (0.5 m deep) the reflectivity of the bed can be bright enough that 17–20% of the transmitted solar radiation can be lost back to the atmosphere, whereas that proportion declines to about 7–9% in a 5 m

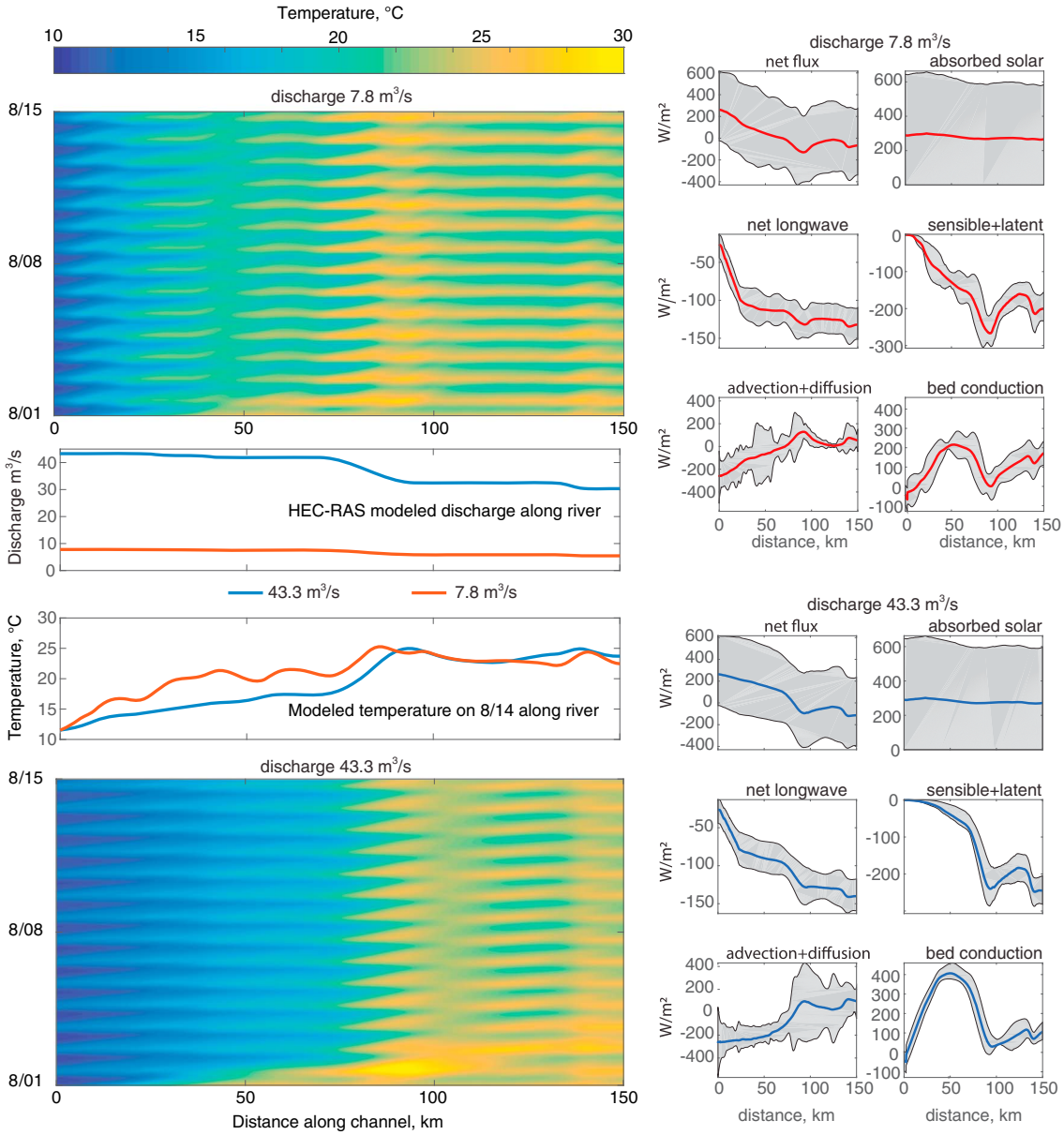

Figure 3. Predicted *T* (left) and mean and interquartile range of energy fluxes (right) for a steady state discharge of 7.8 $m^3\ s^{-1}$ (275 cubic feet per second (cfs)) and 43.3 $m^3\ s^{-1}$ (1530 cfs) over a length of 150 km during an observed warm summer period (1 August to 15 August 2010). In both flow scenarios, bed albedo is assigned based on observations ranging from gravel (0.08) upstream to sand (0.43) downstream.

deep river. Thus, by accounting for the spectral dependence and calculating the reflectivity R_{back} of the whole system, the analysis shows that a significant proportion of light reflected from the bed escapes back out of the water column. The depth at which differences in sediment cease to influence S_{net} (total absorption by sand and gravel converges to within <5%) is approximately 8 m, depending on sun angle. At this depth, S_{net} becomes independent of sediment type and suggests that traditional predictions, without accounting for the spectral variability in absorption, are most applicable to deep rivers.

Real rivers are not subject to constant flow events and homogenous beds but also to along-stream variations in discharge and sediment. Figure 3 shows that the distance over which differences in discharge influence water temperature is limited to tens of kilometers for both a low flow (7.8 $m^3\ s^{-1}$) and a bankfull flow (43.3 $m^3\ s^{-1}$) and eventually meteorology takes over. The corresponding energy fluxes for the San Joaquin River flow and climate confirm that the net absorption of shortwave radiation is the dominant source of

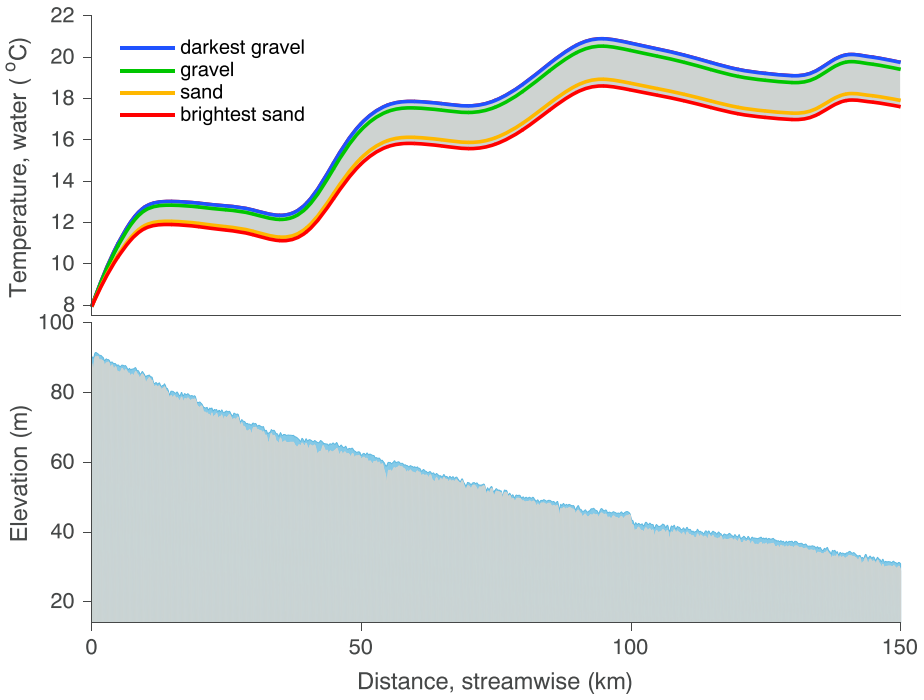

Figure 4. Effects of sediment variations to river temperature (T, °C) over the length of the San Joaquin River for a snapshot in time (24 April 2010 12:00 P.M.), with R_{bed} ranging from dark gravel (0), gravel (0.08), sand (0.43), and bright sand (0.5) for a low flow to bankfull flow D (0.5 m).

heating, while the dominant cooling arises from the net longwave radiation and latent heat flux, which are persistently negative but have steeper streamwise gradients at lower flows. Sensible heat transfer is usually positive, but its magnitude is insufficient to balance the latent heat transfer. Although bed conduction has similar magnitudes to the latent heat transfer, it varies systematically between day and night so the net effect on water temperature is small.

Sand bed rivers transport water that is cooler than gravel bed rivers, and longitudinal variations in sediment alone—particularly along the gravel-sand transition—can reduce T by 1–2°C (Figure 4). For the range of discharges considered here, differences in bed albedo can have a greater influence than changes in flow to Q_{net} and T. The spectral attribute provides a mechanistic basis to explain why sandy beds have a greater resistance to heating than gravelly beds. Results of the model validation show, without calibration, mean biases from −1.0 to +0.8°C and root-mean-square error values from 0.2 to 1.4°C (Table S4 in the supporting information [*Legates and McCabe*, 1999]) when compared with observed T during a 7 day validation period (supporting information).

4. Conclusions

The spectral and fluvial attribute of the energy balance offers several new insights. First, it allows us to formalize a systematic, physically based approach by which to consider some roles of fluvial processes in the energy balance. Second, it provides evidence that sediment albedo is a first-order control to the fluvial energy balance in clear water below dams, and that river temperature depends in part on fluvial processes via the delivery of sediment and the position of the gravel to sand transition. Third, it reveals that for much of the spectrum (beyond 1 μm), the fraction of solar radiation absorbed is independent of river depth. Analysis of the energy balance explains why releases of cold water have a limited influence on river temperature beyond tens of kilometers downstream of a dam.

Acknowledgments
This work was supported by the Delta Stewardship Council Delta Science Program under award number U-04-SC-005. Data used in this article can be obtained from the lead author. E.B., J.D., and T.D. contributed equally to designing the analysis, developing the model, and writing the manuscript. E.B. and J.D. conducted the numerical modeling. Cited references unavailable online can be obtained at www.bren.ucsb.edu/~ebray/references/fluvialEB.

References

Benjamin, J. R., P. J. Connolly, J. G. Romine, and R. W. Perry (2012), Potential effects of changes in temperature and food resources on life history trajectories of juvenile *Oncorhynchus mykiss*, *Trans. Am. Fish. Soc.*, *142*, 208–220, doi:10.1080/00028487.2012.728162.

Blinn, D. W., and G. A. Cole (1991), Algal and invertebrate biota in the Colorado River: Comparison of pre-and post-dam conditions, in *Colorado River Ecology and Dam Management*, edited by National Research Council, pp. 102–123, Natl. Acad. Press, Washington, D. C., doi:10.17226/1832.

Born, M., and E. Wolf (1959), *Principles of Optics*, 614 pp., Pergamon Press, New York.

California Department of Water Resources (2010), CDWR 2009 interim flows data report DRAFT, 3/26/2010. Appendix IV: 34 San Joaquin River Riffle Particle Size Composition Survey Interim Report, River Miles 247–267. Final Draft., California Dep. of Water Resources.

Carbonneau, P. E., and H. Piégay (2012), Introduction: The growing use of imagery in fundamental and applied river sciences, in *Fluvial Remote Sensing for Science and Management*, pp. 1–18, John Wiley, Chichester, U. K., doi:10.1002/9781119940791.ch1.

Constantz, J. (2008), Heat as a tracer to determine streambed water exchanges, *Water Resour. Res.*, *44*, W00D10, doi:10.1029/2008WR006996.

Craine, J. M., N. Fierer, and K. K. McLauchlan (2010), Widespread coupling between the rate and temperature sensitivity of organic matter decay, *Nat. Geosci.*, *3*, 854–857, doi:10.1038/ngeo1009.

Crawford, T. M., and C. E. Duchon (1999), An improved parameterization for estimating effective atmospheric emissivity for use in calculating daytime downwelling longwave radiation, *J. Appl. Meteorol.*, *38*, 474–480, doi:10.1175/1520-0450(1999)038<0474:AIPFEE>2.0.CO;2.

Dozier, J., and S. I. Outcalt (1979), An approach toward energy balance simulation over rugged terrain, *Geogr. Anal.*, *11*, 65–85, doi:10.1111/j.1538-4632.1979.tb00673.x.

Dunne, T., and R. E. Aalto (2013), Large river floodplains, in *Treatise on Geomorphology*, edited by J. F. Shroder, pp. 645–678, Academic Press, New York.

Fischer, H. B., J. E. List, C. R. Koh, J. Imberger, and N. H. Brooks (2013), *Mixing in Inland and Coastal Waters*, 302 pp., Academic Press, New York.

Gueymard, C. A. (2004), The sun's total and spectral irradiance for solar energy applications and solar radiation models, *Sol. Energy*, *76*, 423–453, doi:10.1016/j.solener.2003.08.039.

Hale, G. M., and M. R. Querry (1973), Optical constants of water in the 200-nm to 200-μm wavelength region, *Appl. Opt.*, *12*, 555–563, doi:10.1364/AO.12.000555.

Hausner, M. B., K. P. Wilson, D. B. Gaines, F. Suárez, and S. W. Tyler (2013), The shallow thermal regime of devils hole, Death Valley National Park, *Limnol. Oceanogr. Fluids Environ.*, *3*, 119–138.

Julian, J. P., M. W. Doyle, and E. H. Stanley (2008), Empirical modeling of light availability in rivers, *J. Geophys. Res.*, *113*, G03022, doi:10.1029/2007JG000601.

Kasten, F., and A. T. Young (1989), Revised optical air mass tables and approximation formula, *Appl. Opt.*, *28*, 4735–4738, doi:10.1364/AO.28.004735.

Kirk, J. T. O. (2011), *Light and Photosynthesis in Aquatic Ecosystems*, 3rd ed., 662 pp., Cambridge Univ. Press, New York.

Legates, D. R., and G. J. McCabe Jr. (1999), Evaluating the use of "goodness-of-fit" measures in hydrologic and hydroclimatic model validation, *Water Resour. Res.*, *35*, 233–241, doi:10.1029/1998WR900018.

Legleiter, C. J., D. A. Roberts, and R. L. Lawrence (2009), Spectrally based remote sensing of river bathymetry, *Earth Surf. Processes Landforms*, *34*, 1039–1059.

Leopold, L. B., and M. G. Wolman (1957), *River Channel Patterns: Braided, Meandering, and Straight*, Professional Paper 282-B, p. 50, *U.S. Geological Survey, U.S. Geol. Surv. Prof. Pap., 282-B*, 50 pp., Washington, D. C. [Available at https://pubs.er.usgs.gov/publication/pp282B.]

Paola, C., and P. Wilcock (1989), Downstream fining in gravel bed rivers, *Eos Trans. AGU*, *70*, 852–852, doi:10.1029/89EO00290.

Paola, C., P. L. Heller, and C. L. Angevine (1992), The large-scale dynamics of grain-size variation in alluvial basins, 1: Theory, *Basin Res.*, *4*, 73–90, doi:10.1111/j.1365-2117.1992.tb00145.x.

Prata, A. J. (1996), A new long-wave formula for estimating downward clear-sky radiation at the surface, *Q. J. R. Meteorol. Soc.*, *122*, 1127–1151, doi:10.1002/qj.49712253306.

Richtmyer, R. D., and K. W. Morton (1967), *Difference Methods for Intitial Value Problems*, 2nd ed., 405 pp., John Wiley, New York.

Sellers, W. D. (1965), *Physical Climatology*, 272 pp., Univ. of Chicago Press, Chicago, Ill.

Singer, M. B. (2008), Downstream patterns of bed material grain size in a large, lowland alluvial river subject to low sediment supply, *Water Resour. Res.*, *44*, W12202, doi:10.1029/2008WR007183.

Sridhar, V., A. L. Sansone, J. LaMarche, T. Dubin, and D. P. Lettenmaier (2004), Prediction of stream temperature in forested watersheds, *J. Am. Water Resour. Assoc.*, *40*, 197–213, doi:10.1111/j.1752-1688.2004.tb01019.x.

Verburg, P., and J. P. Antenucci (2010), Persistent unstable atmospheric boundary layer enhances sensible and latent heat loss in a tropical great lake: Lake Tanganyika, *J. Geophys. Res.*, *115*, D11109, doi:10.1029/2009JD012839.

Ward, J. V. (1989), The four-dimensional nature of lotic ecosystems, *J. N. Am. Benthol. Soc.*, *8*, 2–8, doi:10.2307/1467397.

Zeng, Y., and W. Huai (2014), Estimation of longitudinal dispersion coefficient in rivers, *J. Hydrol. Res.*, *8*, 2–8, doi:10.1016/j.jher.2013.02.005.

Zhang, H., and K. J. Voss (2006), Bidirectional reflectance study on dry, wet, and submerged particulate layers: Effects of pore liquid refractive index and translucent particle concentrations, *Appl. Opt.*, *45*, 8753–8763, doi:10.1364/AO.45.008753.